J. Electrochem. Sci. Eng. **13(1)** (2023) 163-172; https://dx.doi.org/10.5599/jese.1431

Open Access : : ISSN 1847-9286
https://pub.iapchem.org/ojs/index.php/JESE

Original scientific paper

Mechanical and microstructural characterization of $YSZ/Al_2O_3/CeO_2$ plasma sprayed coatings

V. V. Satyavathi Yedida and Hitesh Vasudev✉

School of Mechanical Engineering, Lovely Professional University, Phagwara-144411, India

Corresponding author: ✉hiteshvasudev@yahoo.in

Received: June 29, 2022; Accepted: July 7, 2022; Published: September 6, 2022

Abstract

In the present work, the surface characterization of $YSZ/Al_2O_3/CeO_2$ plasma sprayed coatings was performed to understand the surface characteristics. The content of the Yttria-stabilized zirconia (YSZ) was 60 wt.% , where alumina was varied from 30 to 38 wt.% and CeO_2 from 2 to 10 wt.%, respectively. Ceramic coatings with a different variation of composite materials were used to increase layer strength on a substrate of SS-304. The SEM micrographs were analysed to understand the features present on the surface of coatings, and XRD analysis was done to ascertain the phases present in the coatings. Microhardness and porosity decrease with the addition of CeO_2 in the YSZ-based coatings.

Keywords

Coatings methods; biomedical implants; tissue engineering

Introduction

The different materials are used nowadays in various applications such as biomaterials ad high-temperature applications. The main purpose of using materials is to get enhanced performance under aggressive conditions. For instance, aluminum oxide (Al_2O_3), often known as alumina, has been used as a material for prostheses and surgical device components since 1970 [1]. It is an inert component with good corrosion resistance in an in vivo environment. Similarly, yttria-stabilized zirconia (YSZ) material is used in thermal barrier coatings and there are other examples exist where a specific class of material is used to counter aggressive conditions. Improved thermal barrier coatings (TBCs) will enable future gas turbines to operate at higher gas temperatures. Considerable effort is being invested, therefore, in identifying new materials with even better performance than the current industry standard, yttria-stabilized zirconia (YSZ). We review recent progress and suggest that an integrated strategy of the experiment, intuitive arguments based on crystallography, and simulation may lead most rapidly to the development of new TBC materials [2]. Designing and developing the best gas turbine engine components exposed to various operating conditions has been quite challenging in the last few decades. Gas turbine components have been traditionally

made of nickel, chromium, cobalt, titanium, and aluminum-based superalloys. Nickel-based superalloys are found to be the best materials to design turbine components. Recently various fields have been researched to improve the efficiency of gas turbines operating in high temperature and harsh environments. Improvement of gas turbine performance includes prolonged operating life, high operating efficiency, and reduced emissions. To satisfy these conditions, increasing thermos-dynamic efficiency by increasing turbine entry temperature is the most effective [3].

To improve the turbine's performance and lifetime, the perfect material must be selected. Initially, the gas turbine engines were designed using various types of stainless steels, but they don't exhibit improved heat resistance. So, stainless steels were replaced by nickel-based superalloys, such as Nimonic or Inconel, which exhibit better heat resistance [4]. A single crystal (SC) casting technology has been introduced to produce single crystal blades. Single crystal blades can be operated at high temperatures compared to directional solidification blades. However, at very high temperatures, core parts will damage if exposed directly without any thermal barrier. So, a TBC is applied to the gas turbine parts directly exposed to the high-temperature environment from 1370-1590 °C. By applying low thermal conductivity coating on gas turbine blades, the temperature of the components can be reduced by approximately 100-300 °C [5]. Using this technique, the gas turbine can be operated at a combustion gas temperature 250 °C higher than the melting temperature of nickel-based superalloys. TBCs also increase the service life because they reduce the temperature of metal components.

In the present work, the surface characterization of YSZ/Al_2O_3/CeO_2 plasma sprayed coatings has been performed to understand the surface characteristics. YSZ with 60 % and alumina varied from 30 to 38 % and CeO_2 from 2 to 10 %. Ceramic coatings with a different percentage variation of composite materials are used to increase layer strength on a substrate of SS-304. Stainless steel grade is used in various biomedical and high-temperature applications. The SEM micrographs were analysed to understand the features present on the surface of coatings and XRD analysis was done to know the phases present in the coatings.

Methodology and materials

The present work is aimed at the deposition of YSZ/Al_2O_3/CeO_2 coatings by using plasma spraying process. The deposition of the coating is followed by the mechanical and microstructural characterization of YSZ/Al_2O_3/CeO_2 plasma sprayed coatings

Preparation of substrate material

The stainless-steel SS-304 as substrate material in form of flat plate was purchased from Bharat Aerospace Metals, Mumbai, having dimensions 300×200×5 mm^3 and the plate was then further cut using a wire-cut electro discharge machine (WEDM) as shown in Figure 1. YSZ, Al_2O_3 and CeO_2 powders were utilized for preparing the composite powders. Thereafter specimens were polished down to 1200 emery paper grade. The composition of the SS-304 was confirmed by using optical spectrometer.

Figure 1. *SS-304 substrates obtained after WEDM cutting*

The polished samples were grit blasted with 16 mesh size alumina in a grit blasting machine (Model: MEC-9182) with a blasting pressure of 49,000 Pa. The equipment and the medium used for grit blasting are presented in Figure 2. Average surface roughness (R_a) of 6µm was maintained to ensure the proper mechanical anchorage of the coating powder with the substrate. The powders were mixed prior to the deposition of coatings in a ball mill for 4 h using steel balls at 450 rpm.

Figure 2. *(a) Front and (b) side view of shot blasting machine and (c) blasting medium*

The deposited coatings showed a whitish appearance, as shown in Figure 3. However, after a few days from the deposition of coatings, the color of the coatings has turned into a yellowish shade. The designation system used for the coatings is shown in Figure 2. This table shows the content of coating powders used for the deposition of coatings.

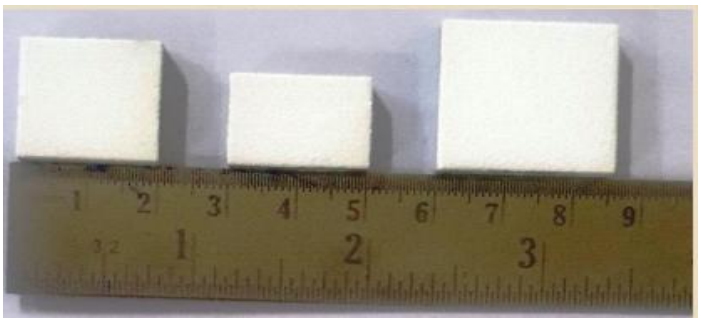

Figure 3. *Macrographs of coated samples*

Table 1. *Plasma spray process parameters employed for deposition of composite coatings*

Parameters selected for spraying	NiCrAlY	YSZ	Top coats
Power, W	30	40	35
Current, A	500	703	560
Voltage, V	60	57	63
Primary gas flow, standard liter per minute	110	85	100
Secondary gas flow, standard liter per minute	11	15	15
Stand off distance (SOD), m	135	100	120
Powder feed rate, g min^{-1}	13	20	13-15
Substrate pre-heat temperature, °C	150	200	200-250

Table 2. *System followed for designation of composite coatings*

Designation	Content, wt.%		
	YSZ	Al_2O_3	CeO_2
Coating 1	100	-	-
Coating 2	60	38	2
Coating 3	60	34	6
Coating 4	60	30	10

The cross-sectional porosity analysis was performed on the acquired optical images of the coating with the help of an image analysis software, *Dewinter Material Plus, Version 4.3*. A total of ten readings were taken at different locations along the cross-section of the developed coating for porosity measurements. Finally, the average values of microhardness and porosity measurements were reported for the developed coating.

Results and discussion

The SEM micrographs of the feedstock powders are shown in Figure 3. FE-SEM images of the YSZ, Al_2O_3, NiCrAlY and CeO_2 powders were used for the composite coatings.The average size of all the spherical powder agglomerates was observed to be in the range of 40-70 µm.

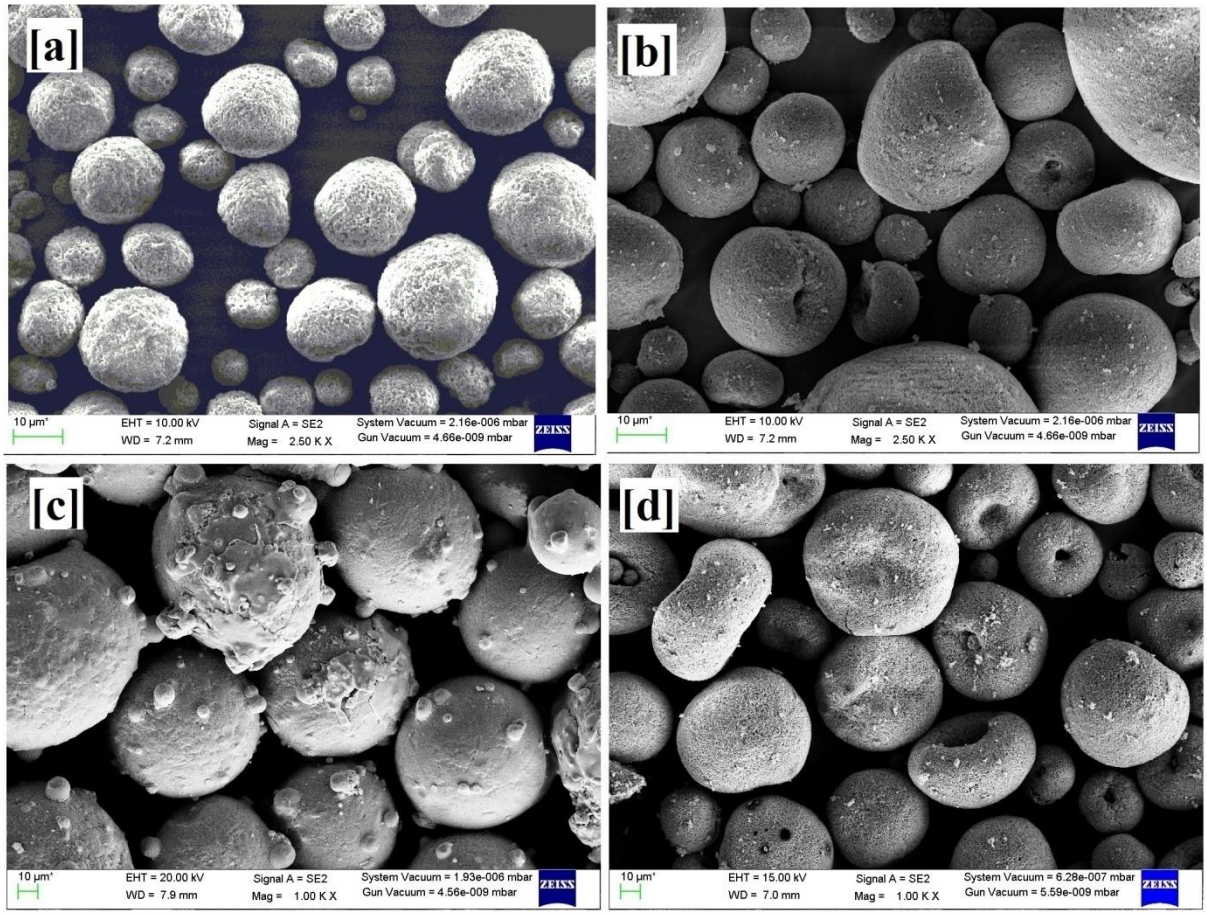

Figure 3. *FE-SEM images of (a) YSZ, (b) Al_2O_3, (c) NiCrAlY and (d) CeO_2 powders*

Figure 4 shows the XRD pattern of the obtained YSZ, Al_2O_3, and CeO_2 powders, respectively. It can be seen that all the peaks of the YSZ powder show the tetragonal phase. The XRD spectra of Al_2O_3 powders showed only the characteristic peak of α- Al_2O_3 phase. Similarly, the XRD spectra of CeO_2 powders show the presence of only the cubic CeO_2 phase.

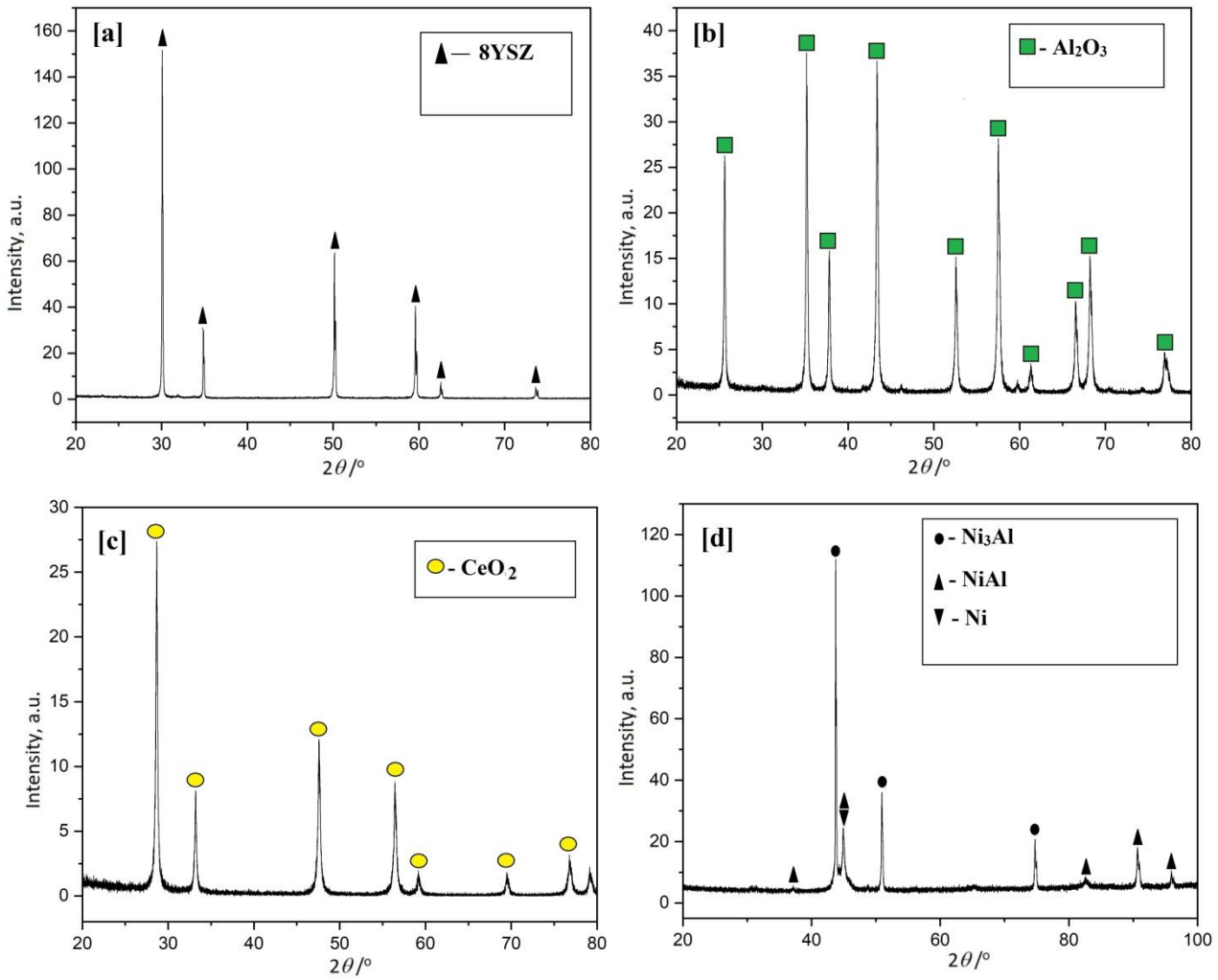

Figure 4. *XRD patterns of (a) YSZ, (b) Al_2O_3, (c) CeO_2 and (d) NiCrAlY powders*

Figure 5 shows micrographs of top surfaces of as-sprayed YSZ coating (coating 1). Figures 5a and 5b display the top surface morphology of as-sprayed YSZ coating at higher magnification [13000x]. Micrographs clearly indicate that during spraying, droplets less than <1 µm were formed and deposited. The SEM micrograph with a high magnification level corresponding to Figure 5a has been shown in Figure 5b [6]. Nano-sized (<1 µm) solidified droplets can be seen in Figures 5b and 5c. The top surface of the coating also shows a large porosity (Figures 5a and 5b) which is beneficial for hot section parts of the gas turbine engine. Energy dispersive spectroscopy (EDS) corresponds to the elements present in YSZ coating, as presented in Figure 5c. Another set of SEM-EDS analysis was done for coating 1 to understand the microstructural features of coating 1. The coatings were characterized for the as-sprayed surface, and chemical composition and elemental distribution were checked. Figure 6a represents the SEM micrograph of YSZ coating (coating 1).The coatings shows the typical features of plasma spray coatings. The features involve melted and unmelted particles. Figure 6b represents the SEM micrograph of YSZ coating (coating 1) at higher magnification, where the well-distributed structure can be observed and EDS was taken, corresponding to Figure 6b. EDS analysis confirms the presence of Zr, Y and O in the coatings, as shown in Figure 6c [7].

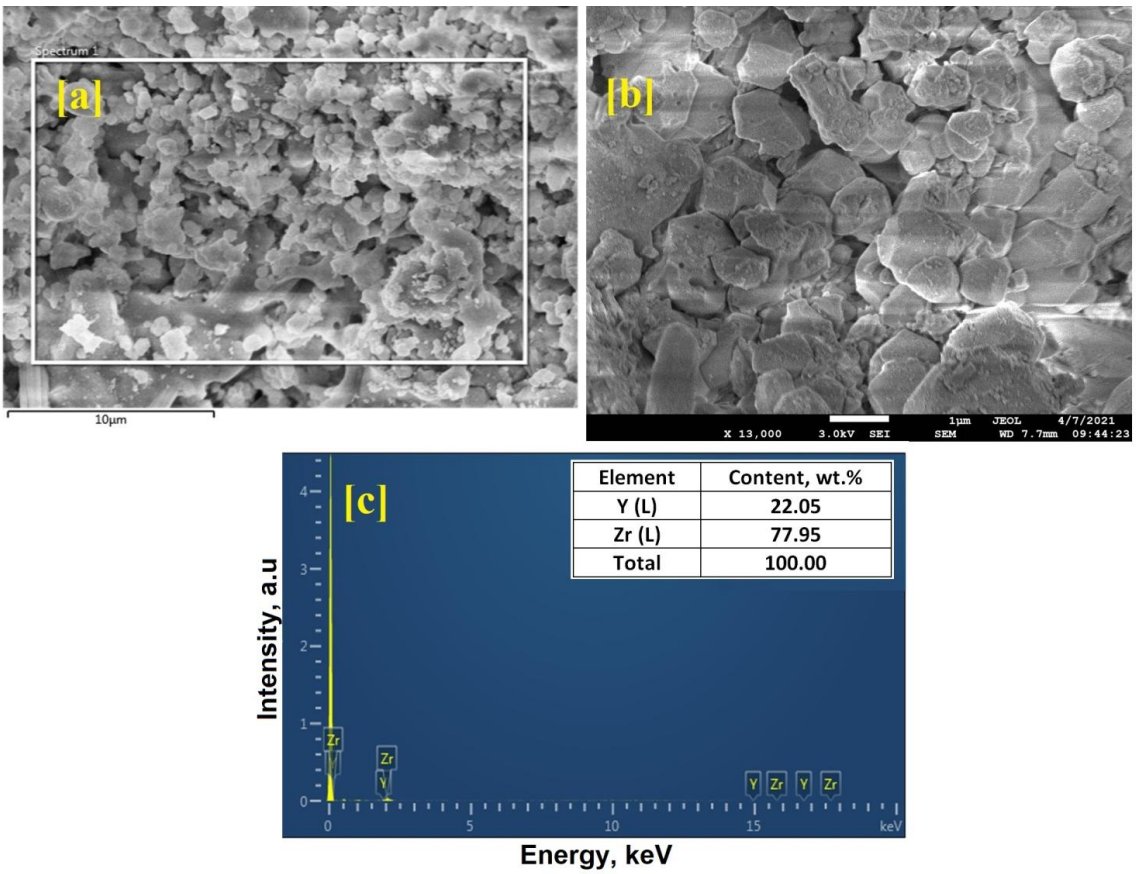

Figure 5. *FE-SEM images of the (a) YSZ coating (coating 1) at low magnification level; (b) YSZ coating (coating 1) at higher magnification level and (c) EDS of coating corresponding to rectangle in (a)*

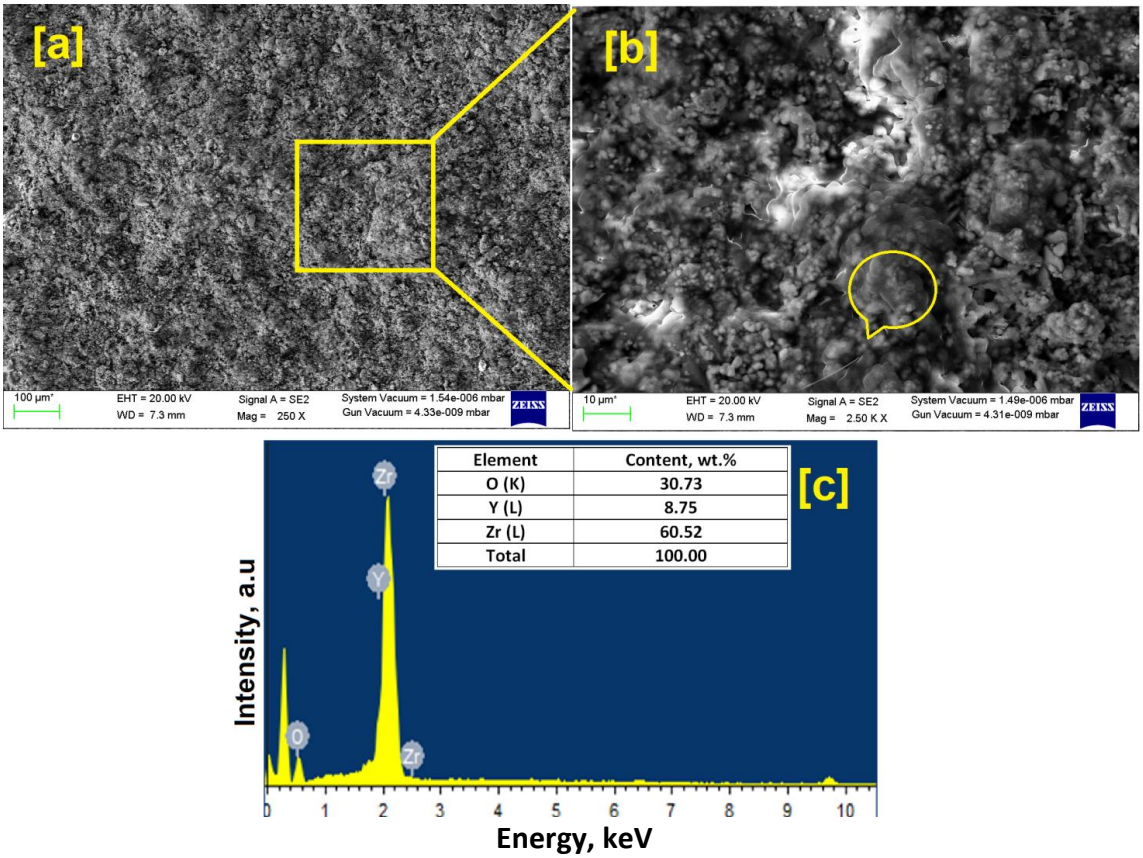

Figure 6. *(a) SEM micrograph of YSZ coating (coating 1), (b) SEM micrograph of YSZ coating (coating 1) and (c) EDS corresponding to (b)*

Figure 7a represents the SEM micrograph of YSZ-based coating (coating 2). The coating surface shows the characteristics of the plasma spraying technique. The surface morphology of coating 3 showed the distributed particles on the surface. The surface is composed of a melted zone and an unmelted zone. Figure 7b represents the particles of Ce embedded on the surface and the same has been confirmed by taking EDS corresponding to Figure 7b [8]. EDS analysis confirms the increase of Ce and O content in coating 2, as shown in Figure 7c.

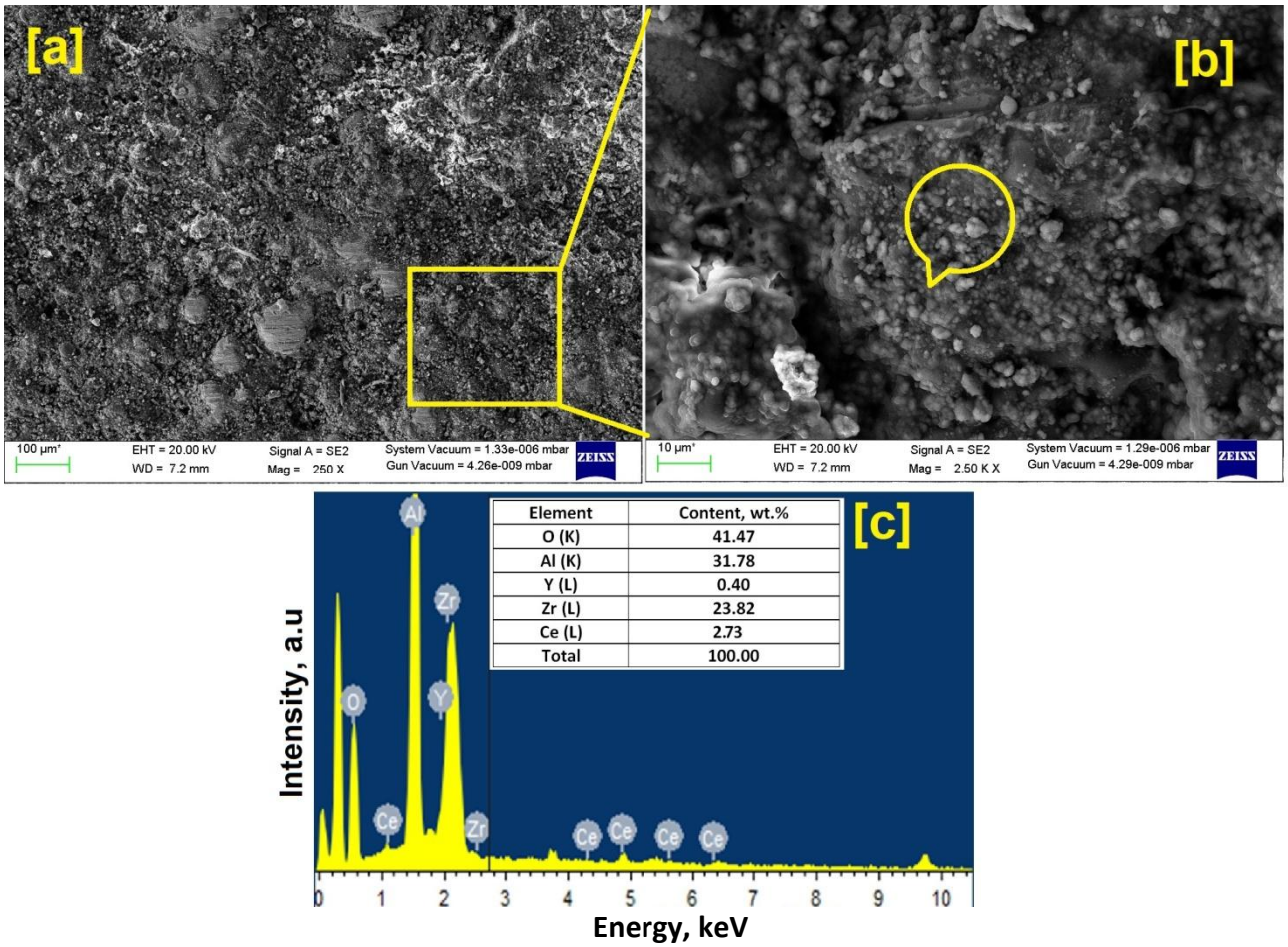

Figure 7. *(a) SEM micrograph of YSZ-based coating (coating 3), (b) SEM micrograph of coating 3 and (c) EDS corresponding to (b)*

Figure 8a represents the SEM micrograph of YSZ-based coating (coating 4). The surface topography represents the formation of ceramic un-melted clusters on the surface Figure 8b represents the uniform distribution of ceramic particles throughout the SEM micrograph and EDS was taken corresponding to Figure 8b to confirm the composition of coating 4. EDS analysis confirms the surge in Ce and O in the coatings corresponding to the combination prepared by adding different feedstock's for coating 4 as shown in Figure 9c. The intensity of CeO_2 has increased with an increase in the content of Ce. The same can be observed in Figure 10, where the maximum intensity of CeO_2 was observed.

The XRD patterns of the deposited coatings can be observed in Figure 10. The tetragonal phase was formed in YSZ coating. The t-ZrO_2 can be observed in Figure 10a. The XRD patterns of the other deposited coatings show the t-ZrO_2, α- Al_2O_3 and CeO_2 [9]. The intensity of the phases has increased for CeO_2 in the coatings by 6 and 10 %.

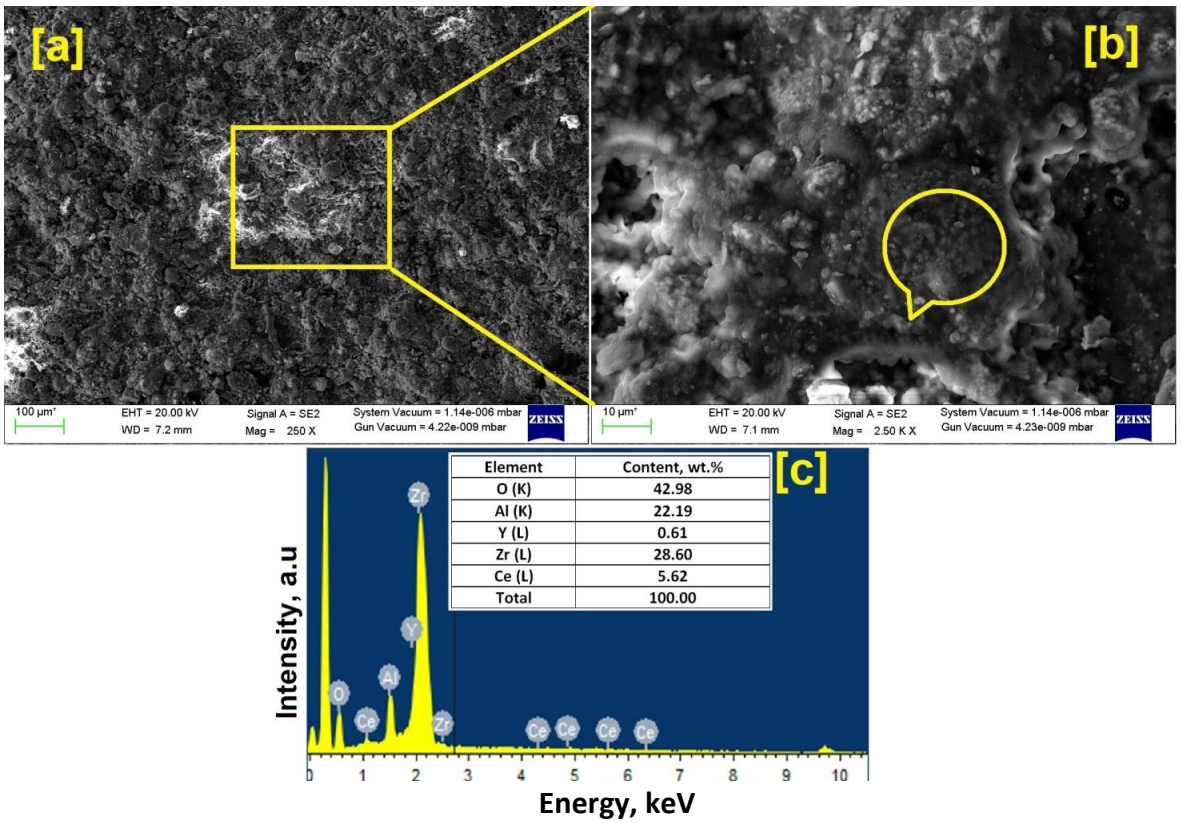

Figure 8. *(a) SEM micrograph of YSZ-based coating (coating 4), (b)SEM micrograph of YSZ-based coating (coating 4) and (c) EDS corresponding to (b)*

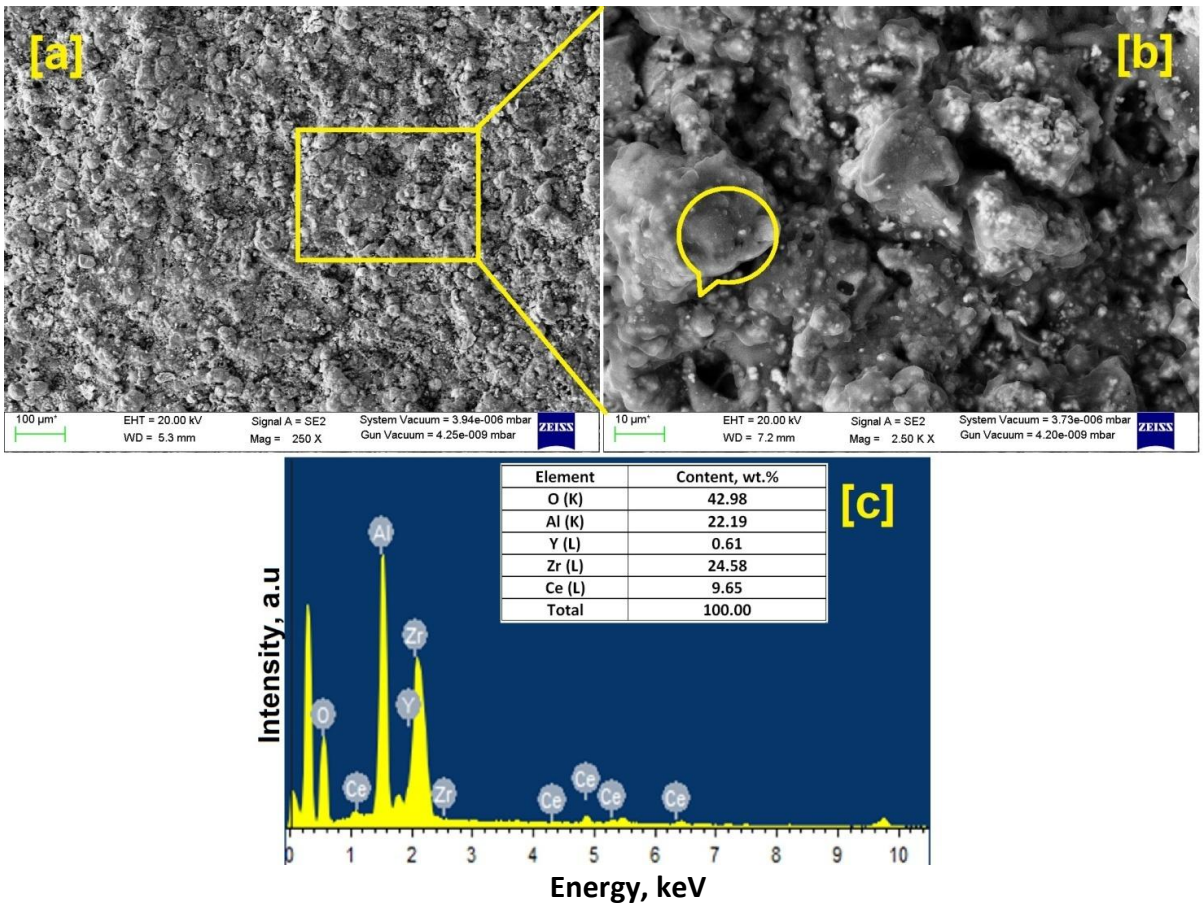

Figure 9. (a) SEM micrograph of coating 4, (b) SEM micrograph of YSZ and (c) EDS corresponding to (b)

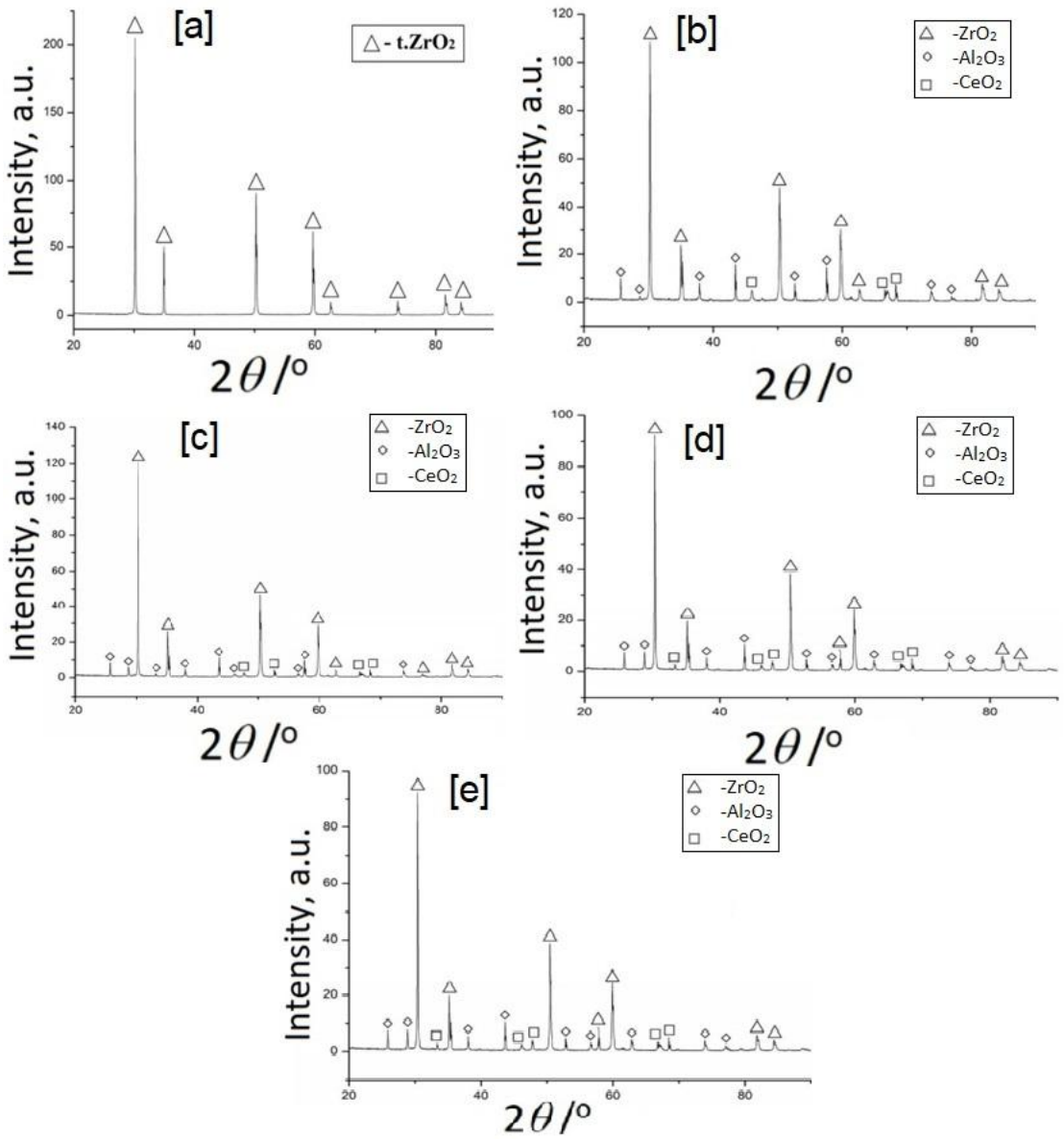

Figure 10. *(a) XRD of YSZ plasma sprayed coating, (b) XRD of 60 % YSZ + 38 % Al_2O_3 + 2 % CeO_2, (c) XRD of 60 % YSZ + 34 % Al_2O_3 + 6 % CeO_2, (d) XRD of 60 % YSZ + 30 % Al_2O_3 + 10 % CeO_2 and (e) XRD of 60 % YSZ + 30 % Al_2O_3 + 10 % CeO_2*

Microhardness test

The microhardness (MH) test was performed at 300 g load for a dwell period of 15 s. The microhardness test was performed at Vickers microhardness tester. An average of five readings has been reported in this article, as shown in Table. 3.

Table 3. *Microhardness and porosity measurements of composite coatings*

Designation	Content, wt.%			Microhardness, HV
	YSZ	Al_2O_3	CeO_2	
Coating 1	100	-	-	1256 ± 10
Coating 2	60	38	2	1130 ± 12
Coating 3	60	34	6	1025 ± 12
Coating 4	60	30	10	951 ± 10

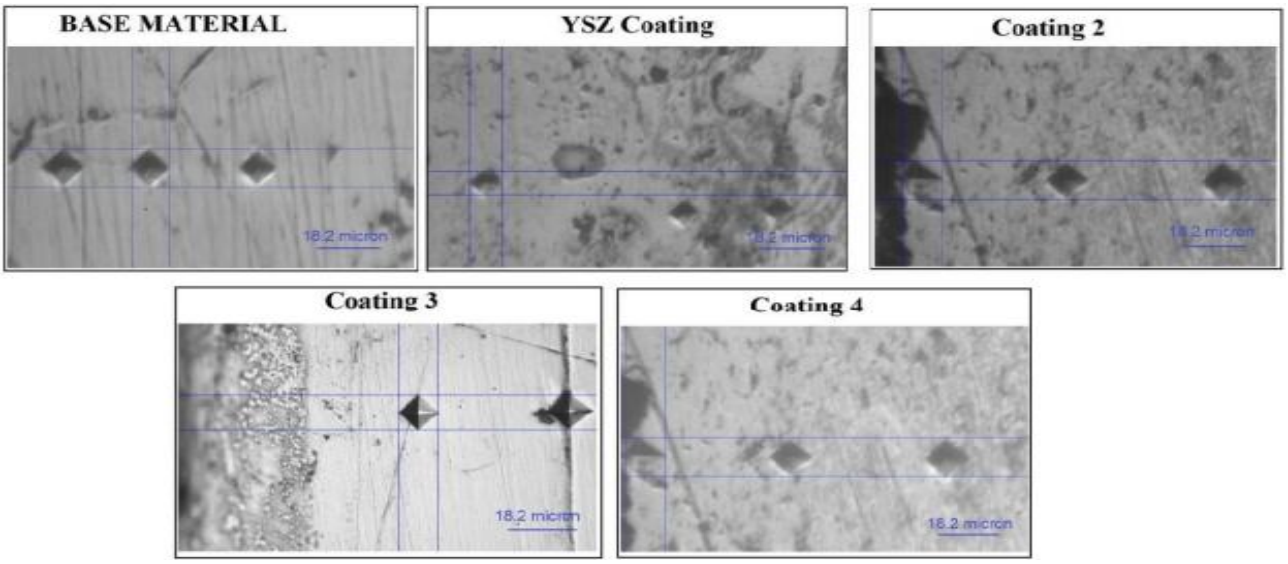

Figure 11. *Microhardness indents for substrate and different coatings*

Conclusions

The following conclusions have been drawn from this study:

- Experimental investigation with composite YSZ, Al_2O_3 and CeO_2 coated on SS-304 substrate using atmospheric plasma spray (APS) method by keeping bond coat of 100 µm constantly. The observations from the coatings found that the coating was added uniformly to the surface of the substrate.
- The coating with 10 wt.% CeO_2 showed a good distribution of elements compared to other coatings.
- The YSZ coating showed the highest microhardness of 1256 ± 10 HV, whereas coating with 10 wt.% of CeO_2 was found to be 951 ± 10 HV.

References

[1] I. Bello, C. Y. Chan, W. J. Zhang, Y. M. Chong, K. M. Leung, S. T. Lee, Y. Lifshitz, *Diamond and Related Materials* **14(3-7)** (2005) 1154-1162.https://doi.org/10.1016/j.diamond.2004.12.041

[2] W. Gao, Y. Li, Y. Zhang, H. Yin, *Coatings* **8(2)** (2018) 82. https://doi.org/10.3390/coatings8020082 (retracted: *Coatings* **8(9)** (2018) 316. https://doi.org/10.3390/coatings8090316)

[3] X.W. Zhang, H. Yin, H.G. Boyen, P. Ziemann, M. Ozawa, *Diamond and Related Materials* **14(9)** (2005) 1482-1488.https://doi.org/10.1016/j.diamond.2005.03.001

[4] D. Kapoor, R. Maheshwari, K. Verma, S. P. Sharma,Ghode, R. K. Tekade, *Drug Delivery Systems* (2020) 665-719. https://doi.org/10.1016/b978-0-12-814487-9.00014-4

[5] N. Panich, P. Wangyao, N.Vattanaprateep, S. Yong, *Journal of Metals, Materials and Minerals* **16(2)** (2006) 19-23. http://jmmm.material.chula.ac.th/index.php/jmmm/article/view/257

[6] A. Amanov, T. Watabe, R. Tsuboi, S. Sasaki, *Tribology International* **62** (2013) 49-57. https://doi.org/10.1016/j.triboint.2013.01.020

[7] K. Reichelt, X. Jiang, *Thin Solid Films* **191(1)** (1990) 91-126. https://doi.org/10.1016/0040-6090(90)90277-K

[8] M. D. Allendorf, R. J. Kee, *Journal of the Electrochemical Society* **138(3)** (1991) 841. https://doi.org/10.1149/1.2085688

[9] P. J. Kelly, R. D. Arnell, *Vacuum* **56(3)** (2000) 159-172. https://doi.org/10.1016/S0042-207X(99)00189-X